6558 *Macromolecules* **2009**, *42*, 6558–6563
DOI: 10.1021/ma900924y

Macromolecules
ARTICLE

In-Situ Growing CdS Single-Crystal Nanorods via P3HT Polymer as a Soft Template for Enhancing Photovoltaic Performance

Hung-Chou Liao, San-Yuan Chen,* and Dean-Mo Liu*

Department of Materials Science and Engineering, National Chiao Tung University 1001 Ta-Hsueh Rd. Hsinchu, 30010 Taiwan, Republic of China

Received April 28, 2009; Revised Manuscript Received July 22, 2009

ABSTRACT: A novel method was used to synthesize CdS single-crystal nanorods directly in the presence of conjugated polymer poly(3-hexylthiophene-2,5-diyl) (P3HT), where the P3HT is acting as a molecular template for geometrical manipulation of CdS nanocrystals and, in the meantime, as an efficient charge conductor in composite form. Such a templating process allows the CdS nanorods with various aspect ratios to be easily manufactured via a controlled solvency of a cosolvent mixture, under which the conformational variation of the P3HT chain can be manipulated. The mechanism of in situ growth of high-aspect-ratio CdS nanorod is proposed based on spectroscopic analysis. A considerably improved PL quenching was detected for the nanorods and suggested a result of electronic coupling between the high-aspect-ratio CdS nanorods and the conducting polymer matrix. A photovoltaic device consisting of CdS nanorods with aspect ratio of ca. 16 and the conjugated polymer poly(3-hexylthiophene) was well assembled and showed a power conversion efficiency of as high as 2.9% under air mass (AM) 1.5 global solar conditions.

Introduction

Optoelectronic devices based upon conducting polymers and inorganic nanocrystals are widely studied as type II bulk heterojunctions[1−5] because nanocrystals can act as electron acceptors to assist charge separation and broaden the spectral response. Creating these materials with well-defined physical and electronic properties is an important step toward building type II bulk heterojunctions. Various high electron affinity inorganic semiconductors including CdSe,[3] ZnO,[6] CdTe,[7] and TiO_2[8] have been widely studied for bulk heterojunction polymer solar cells. However, few studies have been reported for utilization of CdS as an important II−VI semiconductor in nanocrystal−conjugated polymer composites, probably due to the relatively large band gap (2.42 eV) that absorbs light ranging from 300 to 512 nm and mismatches with the solar terrestrial radiation (300−1500 nm). Among them the highest power conversion efficiency for a CdS/polymer hybrid solar cell was reported by Wang et al., who fabricated a hybrid solar cell with MEH−PPV and CdS nanorods with a diameter of 3.5 nm and length of 35 nm and obtained a power conversion efficiency of 1.17%.[9] However, since CdS has high electron mobility and the conduction band edge is more negative than the H_2O/H_2 redox potential,[10] it is believed that there has much room for further improvement in the conversion efficiency for hybrid CdS/conjugated polymer photovoltaic devices.

The conventional method for preparing a nanocrystal−conjugated polymer composite is by mixing a given polymer with nanocrystals through the use of surfactants, where the surfactants would form an insulating interface, even in a nanometric length, between the polymer matrix and the nanocrystals, further deteriorating charge transfer ability.[2,3] A variety of methods exists in the literature for the synthesis of ligand-capped metal chalcogenide nanocrystals with controlled size and shape.[11−13] Although the incorporation of the surface ligands into an organic/inorganic composite can improve distribution of nanocrystals in a conjugated polymer, two significant drawbacks ruin the efficiency considerably. First, the ligands inhibit charge transfer between the polymer and the nanocrystals.[4] Second, mixing pyridine-capped nanocrystals and polymer requires the use of cosolvent, which can adversely affect nanocrystal solubility and polymer chain orientation. These problems can be bypassed by directly growing nanocrystals in a conducting polymer solution without surfactants or ligands.[5,14] As demonstrated in an early report, an in situ synthetic method was employed to synthesize PbS nanocrystals/MEH−PPV composite and showed that the polymer chains can act sterically to stabilize nanocrystal growth in solution.[14,15] Up to now, only a few reports were related to the polymer template-directed synthesis of semiconductor nanowires, with notable examples including microchannels within a thin polymer film,[16] a polymer-assisted solvothermal process,[17−19] and mesoscale structures self-assembled from AB or ABC block copolymers.[20,21] It is generally believed that the in situ formation of 1-D nanostructures, e.g., nanorods, in the composite is technically desirable for photovoltaic application because 1-D nanostructures exhibit much better connectivity than spherical nanoparticles and act as large surface area electron acceptors in a bulk heterojunction.[3] In addition, the nanorods are confined in two dimensions modifying the band structure, which results in a tunable optical absorption edge[3] while allowing exciton diffusion and separation along the unconfined dimension.[22] As reported by Sun et al., the CdSe nanorod/polymer hybrid solar cell with a power conversion efficiency of 2.6% can be obtained by mixing CdSe nanorods with an aspect ratio of 13 with P3HT.[23]This also proved that the efficiency of hybrid photovoltaic devices can be improved by using nanocrystals with a higher aspect ratio. However, ligands that inhibit charge transfer still existed between the polymer and the nanocrystals. Therefore, development of semiconductor nanorods with high aspect ratio, without the use of surfactants and/or ligands, should be more technically interesting with improved power-conversion efficiency for a quantum-dot-based photovoltaic device. Here, we report the synthesis of

*Corresponding authors. E-mail: sanyuanchen@mail.nctu.edu.tw (S.-Y.C.), deanmo_liu@yahoo.ca (D.-M.L.).

 Published on Web 08/07/2009

one-dimensional CdS nanocrystals with various aspect ratios in the presence of conducting polymer head-to-tail (HT) poly-(3-hexylthiophene-2,5-diyl) (P3HT). The HT-P3HT can access a low-energy planar conformation, leading to highly conjugated polymers that provide flat, stacking macromolecular structures that allow self-assembly, providing efficient interchain and intrachain conductivity pathways. Moreover, the choice of solvent gives an impact on the extent to which the P3HT chains straighten out. Other study[24] found that the chains are initially rather coiled up, and the extent to which they uncoiled to form straight structures varies strongly with the choice of solvent. Poor solvents lead to chains with a much shorter average hydrodynamic coil radius in solution. In the case of P3HT, the addition of a minor amount of a poor solvent (e.g., methanol) to the solution of P3HT in a good solvent (e.g., chloroform) is accompanied by solvatochromic transition which was explained by Rughooputh et al.[25] as a rod-to-coil transition (stretched structure to ring structure). Therefore, the physical conformation of P3HT chains is affected by solvents. Since the conformational change of the sulfur-bearing P3HT macromolecule may be manipulated via a cosolvent method, the molecular structure of the resulting P3HT can be tunable with various conformations, e.g., from highly tangled coil to elongated or straightened conformation. If this is what is expected, the exposed sulfur atoms along the backbone of the P3HT to the environment may provide anchorage sites for CdS to nucleate and growth. The P3HT is then used as a dual function macromolecule that is acting as a structure-directing template to manipulate the geometrical development of CdS nanocrystals and, in the meantime, becoming an efficient photoelectron conductor when the final CdS−P3HT composite structure can be well constructed, which, to our best knowledge, is designed for the first time and is highly plausible for solar cell application.

Experiment

Materials. Cadmium acetate dihydrate (Sigma-Aldrich, analytic grade) and sulfur (Fluka, analytical grade) were employed as the precursors for CdS formation. Dichlorobenzene (DCB, Sigma-Aldrich, anhydrous) and dimethyl sulfoxide (DMSO, Sigma-Aldrich, analytical grade) were used as the solvents for CdS formation. Poly(3-hexylthiophene-2,5-diyl) (P3HT, Sigma-Aldrich) is electronic grade and regioregular (>98% head-to-tail). Poly(3,4-ethylene dioxythiophene) doped with poly-(styrenesulfonic acid) (PEDOT:PSS, Sigma-Aldrich) was used to improved smoothness of the electrode/active layer contact.

CdS−P3HT Synthesis. In a three-neck round-bottom flask equipped with a magnetic stirring bar and condenser, 8 mL of DCB, 4 mL of DMSO, 0.01 g of cadmium acetate dihydrate, and 0.01 g of P3HT were heated to 100 °C and degassed with nitrogen for 30 min. In a second vial, 0.002 g of sulfur was dissolved in 1 mL of anhydrous DCB. Both solutions were heated to the temperature of the reaction (between 120 and 180 °C) depending on the composite. Then, 1 mL of the sulfur solution was then injected swiftly into the cadmium precursor solution. The solution was allowed to react for 30 min. The mixture of CdS and conducting polymer was purified by removing any cadmium, sulfur ions, and DMSO via adding anhydrous methanol to form the precipitate. After centrifugation, the supernatant was then removed and the composite dissolved in DCB.

Fabrication and Measurement of Device. The indium tin oxide (ITO)-coated glass glass was purchased from Merck, and the resistivity is 10 ohms/sq. The ITO-coated glass was precleaned (DI water, acetone, ethanol, and isopropyl alcohol) and treated with oxygen plasma prior to use. The PEDOT:PSS layer (50 nm) was spin-coated at 2000 rpm and annealed at 120 °C for 30 min. The CdS/P3HT layers (200 nm) were spin-coated from their corresponding dichlorobenzene solutions (30 mg/mL) at 1500 rpm and annealed at 150 °C for 60 min, followed by thermal evaporation of an aluminum electrode. Aluminum top electrodes (100 nm) were deposited by thermal evaporation through a shadow mask, resulting in individual devices with 0.1 cm^2 nominal area. Power efficiency measurements under approximately AM1.5G conditions (100 mW/cm^2) were performed using a xenon lamp-based Newport 91160 W solar simulator. $J-V$ characteristics were measured using a Keithley 2400 electrometer. A Si photodiode (Hamamatsu S1133) was used to check the uniformity of the area exposed. The spectrum of the solar simulator was calibrated using a PV measurement (PVM-154) mono-Si solar cell (NREL calibrated). Reported efficiencies are obtained from an average value of four measurements from a set of four regions on each substrate. These data points are representative of the defect-free device performance and reflect the generally observed trend.

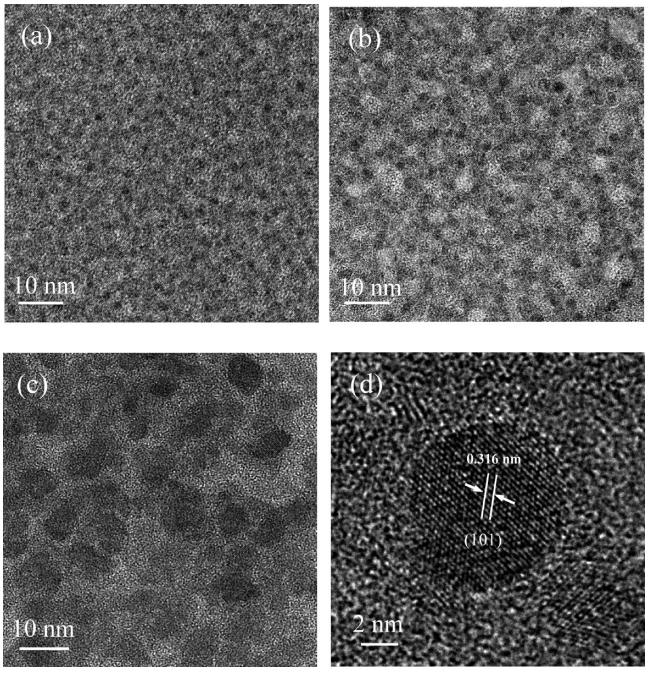

Figure 1. TEM images of CdS nanocrystal ensembles taken at (a) 120, (b) 150, and (c) 180 °C. (d) HRTEM image of the lattice planes in a single CdS nanocrystal.

Structural and Optical Properties Analysis. To investigate the nanostructure of the CdS−P3HT composites, transmission electron microscopy (TEM; JEOL, JEM-2100F, field emission transmission electron microscope) was employed. For TEM images, TEM samples were prepared by immersing carbon grids in composite solutions, and the particle size, particle distribution, and nanostructure of the CdS in the composites can be examined at an operating voltage of 200 kV. The Fourier transfer infrared spectrophotometer (FTIR, PerkinElmer Spectrum 100 spectrometer) was used to identify the chemical structure of materials. Reaction solution was dropped on a KBr plate for analysis. Optical properties were analyzed by UV−vis spectroscopy and a fluorescence spectrometer (Hitachi F4500) equipped with an excitation source of 450 nm wavelength. All films were drop-cast, and care was taken to ensure identical processing of all films. The pristine P3HT film was made from solution which underwent the same processing steps (without adding cadmium acetate and sulfur) with the same polymer concentration.

Results and Discussion

Figures 1a−c show the transmission electron microscopy (TEM) images of the nanocrystals taken at 120, 150, and 180 °C, respectively. It was found that the size of the nanocrystals was increased with the reaction temperature. High-resolution

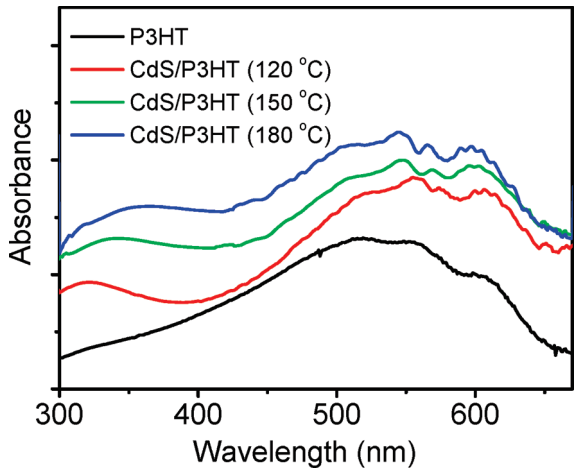

Figure 2. Absorption spectra for P3HT film and a CdS/P3HT composite film synthesized at 120, 150, and 180 °C.

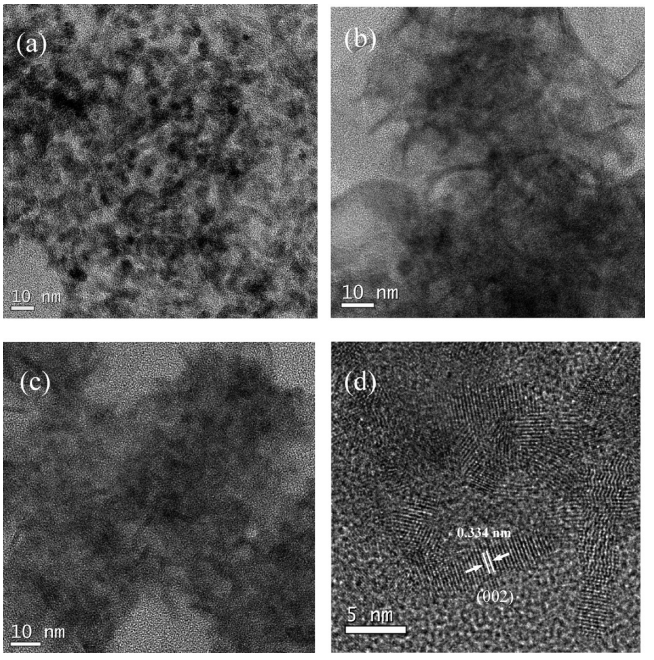

Figure 3. TEM images of CdS nanorods synthesized in P3HT with cadmium acetate concentration of (a) 2.5, (b) 8.3, and (c) 12.45 mg/mL. (d) HRTEM image of the nanorod.

transmission electron microscopy (HRTEM) image (Figure 1d) shows well-developed lattice fringes of the nanocrystals synthesized at 180 °C, indicating the nanocrystals possess high crystallinity. The optical absorption spectrum of a pure P3HT film has an absorption peak at ca. 400 nm in the visible region, and the UV−vis absorption spectra of CdS/P3HT composite film obtained at 120, 150, and 180 °C show the exciton peak behind the polymer exciton absorption peak at ca. 400 nm due to the presence of CdS nanocrystals, as shown in Figure 2. In addition, a red shift in the absorption edge was observed because of the increased size of the nanocrystals with the increase of the reaction temperature.

To better understand the in situ formation of CdS, the influence of reaction parameters, including the concentration of cadmium acetate (and sulfur) and the DCB-to-DMSO ratio, on the in situ reaction was investigated. Figure 3 shows the TEM images of CdS/P3HT samples prepared at different concentrations of cadmium acetate at 180 °C with DCB-to-DMSO ratio of 8:4. When the concentration of cadmium acetate increases to 2.5 mg/mL, CdS nanorods are formed accompanied by CdS nanocrystals, as shown in Figure 3a. As the concentration increases to 8.3 mg/mL, the amount of nanorods also increases, and the nanorods become dominant in this condition as illustrated in Figure 3b. For the sample synthesized from 8.3 mg/mL, the diameter of the nanorods is almost the same as that of samples prepared from 2.5 mg/mL, but the aspect ratio increases to ~8. However, while the concentration exceeded 8.3 mg/mL (i.e., 12.45 mg/mL), except for the formation of the nanorods, nanocrystals (i.e., defined as the ones with equiaxial dimension) are simultaneously observed (Figure 3c), indicating there exists a critical concentration for the nanorod to evolve. The HRTEM image of a single nanorod (appears in Figure 3b) is illustrated in Figure 3d, which confirms a preferential growth of the CdS nanocrystals via its crystallographical (002) orientation. Moreover, the nanostructural evolution of the nanorod was observed in the presence of the P3HT, suggesting the macromolecule may act as a structure-directing template to assemble the growth of the nanocrystal. These observations indicate that the concentration at 8.3 mg/mL provides optimal reaction conditions for the growth of CdS nanorods, along the templated P3HT molecule, rather than those earlier studies where rodlike structure evolved due to a self-assembly of individual equiaxial nanocrystals through dipole−dipole interactions.[26]

Besides the thermodynamic and kinetic factors controlling the synthesis of inorganic nanorods, we believe that P3HT should play a critical role in directing the growth mechanism. It is well-known that both the size and the shape of many inorganic nanocrystals can be dimensionally tuned in a molecular-to-nanometric scale by employing various organic molecules as capping agents during the synthesis process.[27] In this study, the planar P3HT conformation may provide flat, stacking molecular architecture to guide the growth of CdS nanocrystals in an oriented approach like capping agent. It was found that the morphology of the CdS nanorods is significantly determined by the concentration of cadmium acetate in the starting solution.

In order to further elucidate the role the P3HT in CdS crystal development, a comparison of the FTIR transmission spectrum of before and after adding cadmium acetate in reaction and after the reaction is given in Figure 4a. These characteristic bands in the P3HT are 1506, 1455 (aromatic C=C stretching), 1381 (methyl bending), 1106 (C−S stretching), 818 (aromatic C−H out-of plane), and 722 cm^{-1} (methyl rock). After adding cadmium acetate in the solution, characteristic bands of cadmium acetate molecules are observed at 1560 and 1418 cm^{-1} (carboxylate stretching) which overlapped the characteristic bands in the P3HT (1506, 1455, 1381 cm^{-1}). However, a slightly shifted by 5 wavenumbers, corresponding to 6.4×10^{-4} eV, to a lower energy region of C−S characteristic band is observed in the IR spectrum, after mixing of P3HT and Cd precursor, indicating a reduction of the C−S bond energy. This finding suggests additional intermolecular interaction that is activated at the expense of the original C−S bond energy by, for instance, a slight distortion of electronic cloud of the C−S bond. The origin of such an additional intermolecular interaction most probably results from a strong dipole−dipole or ion−dipole interaction between the Cd^{2+} ions and S atoms, prevailing along the backbone of the P3HT chain. The planar P3HT conformation may provide flat, stacking molecular architecture, as schematically shown in Figure 4b. As such, the Cd^{2+} ions may be immobilized in a confined space within the network structure of the P3HT through the dipole−dipole interaction and stayed in place while subjected to a subsequent nucleation-and-growth process with the adding sulfur ions. This would result in uniformly and randomly distributed CdS nanocrystals and nanorods within

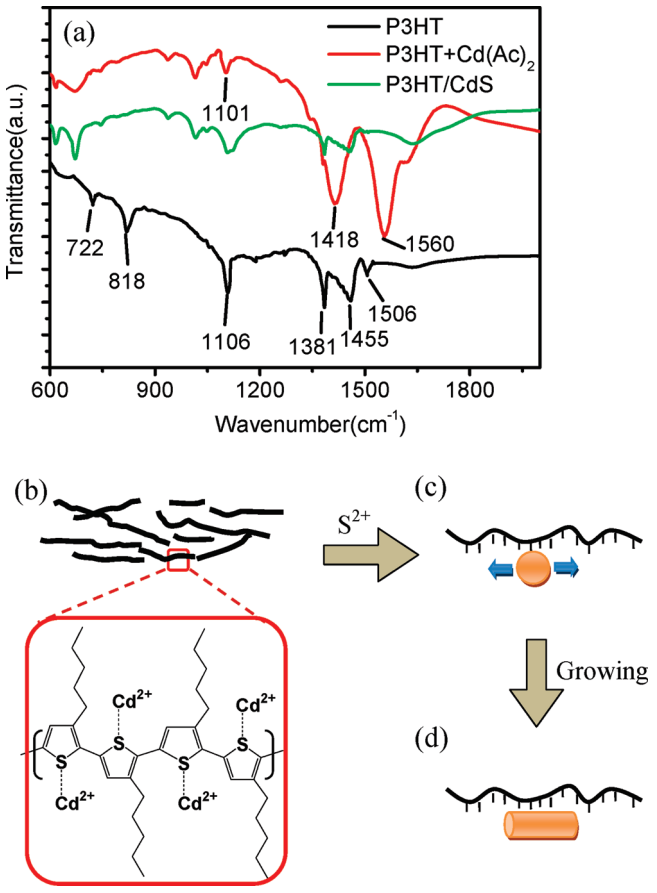

Figure 4. (a) FTIR spectra before and after adding cadmium acetate in reaction and after the reaction. (b) Schematic drawing for the proposed synthesis scheme of CdS/P3HT composite. The Cd^{2+} ions were assumed to be coupled with the unpaired S along the P3HT planar chain network. Proposed mechanism for the growth of (c) CdS nanocrystals and (d) nanorods.

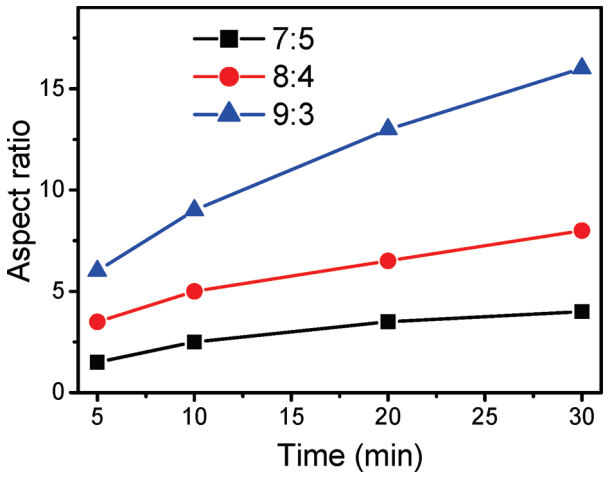

Figure 5. Average aspect ratio of CdS nanocrystals plotted as a function of the reaction time for the CdS nanorods growth.

the polymer, as evidenced in Figures 1 and 3. In order to further prove the hypothesis of this work, we performed a well-controlled experiment. The synthesis was carried out in the absence of P3HT but with the presence of both DCB and DMSO. The resulting nanoparticles were examined using TEM (not shown here), where the obtained nanoparticles showed only equiaxial geometry; in other words, not high-aspect-ratio particles were found. Manoj et al. reported that DMSO can form a complex with Cd during CdS synthesis and results in the formation of capped CdS nanoparticles.[28] However, in this study, no so-called Cd(S)−DMSO complex was formed during reactions according to the results of FTIR spectra. There was not any sign of the absorption peaks originating from DMSO or DCB detected, such as regions at 800 and 1261 cm^{-1} which originated from the Cd(S)−DMSO complex capped CdS nanoparticle itself.

It is known that the high-energy facets grow more quickly than the low-energy facets in a kinetic regime,[27] and the (001) crystal face of CdS has the highest surface energy than all other crystal faces.[29] Consequently, a preferential growth of the CdS nanocrystals along the high-energy facet evolved in the presence of P3HT template, leading to the formation of CdS nanorods. However, if the cadmium acetate concentration is less than 2.5 mg/mL, lower Cd^{2+} ion concentration renders insufficient growth to form a rodlike structure, resulting in formation of equiaxial nanocrystals, as schematically illustrated in Figure 4c. However, with the increase in cadmium acetate concentration, nanorod was successfully developed (Figure 4d). This is due to much more amount of free Cd^{2+} ions available in the solution that allow a subsequent growth of the nanorods by depositing onto the immobilized Cd^{2+} ions along the chain.

The role of structural direction of the P3HT template is essential, since it is assumed, reasonably, that the sulfur atoms along the backbone of the P3HT may act as active sites for Cd^{2+} ions to anchor. Following addition of the sulfur precursor, the sites of Cd^{2+} ion anchorage turn to be the sites for the nucleation and growth of CdS nanocrystal, along the backbone of the P3HT chain, forming CdS nanorod. The single-crystalline nature of the nanorods of various aspect ratios mentioned above suggests an epitaxial-like growth of the CdS nanocrystals along the exposed sulfur-bearing segments of a given macromolecular chain in a given solvent environment. Such a scenario, if molecularly accessible, can be applicable for the nanorods of technically desirable aspect ratio through the manipulation of cosolvent environment where the conformational development of the P3HT polymer can be possible. In other words, an extended and straightened, e.g., in a linear form of, P3HT chain can be evolved if a "good" solvent is applied upon the synthesis of the nanorod. The aspect ratio of the resulting nanorod can be controlled according to the length scale of the P3HT chain that extended into the diluting environment. On this basis, a variation of the DCB-to-DMSO volume ratio from 7:5 to 8:4 to 9:3 gave the nanorods of aspect ratio increasing from 4 to 8 to 16 for the samples with the same concentration under similar reaction conditions. As evidenced from Figure 5, the aspect ratio obtained from the 9:3 ratio was nearly doubled the value compared to that for DCB-to-DMSO of 7:5. Furthermore, it was found that when reaction time is over 30 min, the aspect ratio does not change too much. This demonstrates that a larger ratio of DCB to DMSO can enhances the aspect ratio and growth rate of the nanorods as a result of the conformational variation of P3HT chain in the cosolvent systems. Both structural morphologies of the CdS nanorods synthesized from the 9:3 and 7:5 ratios at 8.3 mg/mL for 30 min are shown in parts a and b of Figure 6, respectively. This indicates that an elongated P3HT chain can be developed upon an increasing DCB-to-DMSO ratio, which corresponds to an increasing CdS size evolution along the (002) direction, resulting in the nanorods with higher aspect ratio. This finding strongly suggests that the templating mechanism of the P3HT macromolecule mentioned above is behaved as a result of a solvent-dependent variation of the polymer chain.

A recent study by Stavrinadis[26] indicated that the PbS nanorods developed from the PbS/MEH−PPV composite are primarily composed of chain of nanocrystals rather than single-crystal nanorod structure. However, in this study, we succeeded in

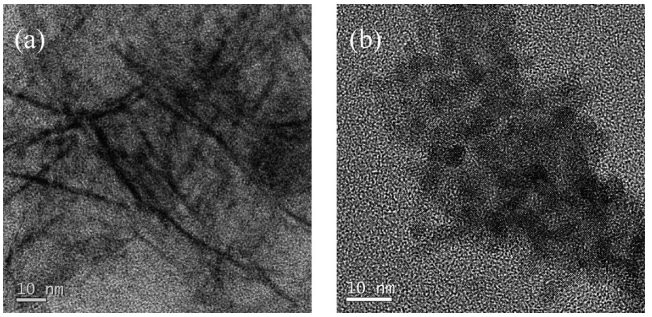

Figure 6. TEM image of CdS nanorods synthesized in P3HT with volume ratio DCB-to-DMSO of (a) 9:3 and (b) 7:5.

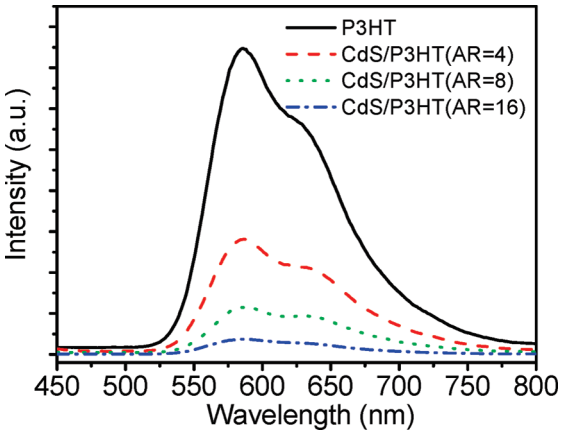

Figure 7. Photoluminescence emission spectra for P3HT and CdS nanorods/P3HT composite solution (both solutions in toluene pumped at 450 nm).

producing CdS single-crystal nanorods in an in situ method. Therefore, it is believed that the growth mechanism of single-crystal nanorod structures is related to P3HT special chain conformation and interchain spacing. In addition, it is well-known that the regioregular, head-to-tail P3HTs can access a low-energy planar conformation, leading to highly conjugated polymers, so we believe that P3HT may act as a molecular template for geometrical manipulation of CdS nanocrystals.

Figure 7 shows the photoluminescence emission spectra of P3HT and CdS/P3HT composites in toluene. In agreement with previous work,[14] a reduction in the spectral intensity of the composites relative to the reference P3HT sample was observed, and the reduction of PL intensity is increased with the aspect ratio of CdS nanorod. This reduction of PL intensity is due to photogenerated charge transfer between the CdS and P3HT.[30] According to previous studies, the decreased photoluminescence intensity of the composites is related to an improvement in photovoltaic performance.[31] The photoluminescence quenching can be also used as a powerful tool for evaluation of charge transfer efficiency in the donor−acceptor blend composites.[32,33] Once the photogenerated excitons are dissociated, the probability for recombination should be significantly reduced. This is a well-known effect of the ultrafast electron transfer from the donor to acceptor, and it is expected to increase the exciton dissociation efficiency in photovoltaic devices.[32−34] Thus, the synthesis of the composites with high-aspect-ratio, single-crystal CdS nanorods provides a significant interest and encourages for further investigations onto the photoconductivity assessment for solar cell use.

Figure 8 gives a summary of operating characteristics for P3HT/CdS-based device using the synthesized CdS nanorods of various aspect ratios. Figure 8a shows the variation of both J_{sc} and V_{oc} with various aspect ratios of CdS nanorods. It was

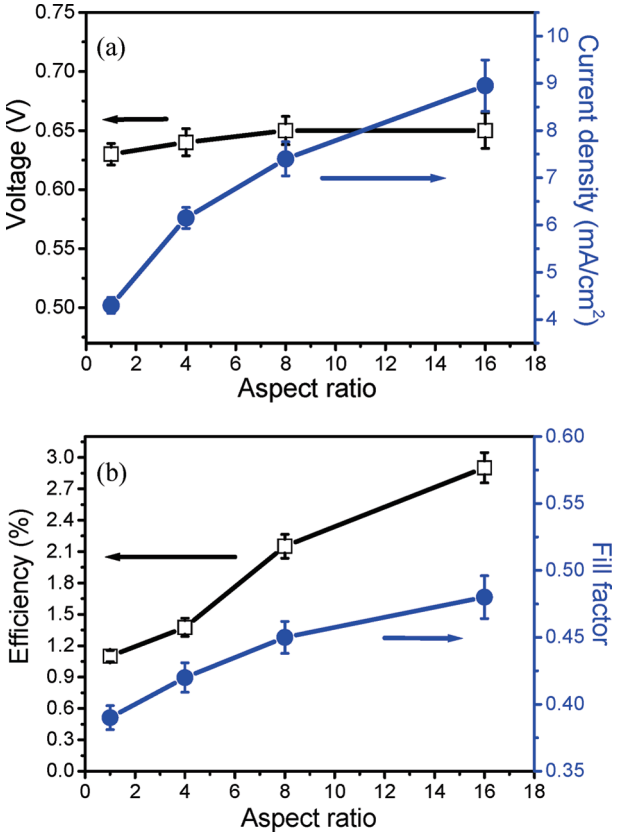

Figure 8. Hybrid solar cell characteristics: (a)V_{oc} and J_{sc}; (b) PCE and FF.

observed that J_{sc} obviously increased with the aspect ratio of the CdS nanorods but V_{oc}, which is limited by the difference between the HOMO of the donor and the LUMO of the acceptor,[35,36] remained identical at ~0.64 V. It suggests a percolation of the CdS forming connective network across the device, rendering the device behaves like a complete heterojunction. The influence of aspect ratio of the CdS nanorods on power conversion efficiency (PCE) and fill factor (FF) is illustrated in Figure 8b. Comparing parts a and b of Figure 8, it can be found that both J_{sc} and FF increased with the aspect ratio of the CdS nanorods, suggesting that the aspect ratio of CdS nanorods reduced charge recombination. The PCE of the well-assembled device using the nanorods with aspect ratio of 16 leads to a considerable improved power conversion efficiency as high as 2.9% due to an increase in both FF and J_{sc}. It was inferred that for the photoactive layers consisting of equiaxial nanoparticles electron transport is dominated by hopping, but the band conduction is prevalent in the photoactive layers consisting of nanorods[3] because the presence of nanorods with high aspect ratio can penetrate through a large portion of the device to develop percolation pathways for electron transport. In other words, longer nanorods are easier to form a percolation path between two electrodes and thereby can thus fully contribute to photovoltaic conversion. Therefore, the increase in PCE and J_{sc} is primarily a result of efficient charge transport.

Conclusion

Formation of CdS nanorods and the corresponding variation of the aspect ratio of the nanorods can be well manipulated via a soft templating technology using the planar P3HT polymer, as a molecular template upon synthesis and, in the meantime, as a conducting matrix to form final P3HT−CdS composite structure, which, to the best of our knowledge, has been explored for

the first time. The formation of the nanorods with various aspect ratios, ranging from ~8 to 16, is controlled by the DCB-to-DMSO ratio of the cosolvent. The nanorods with higher aspect ratio allow connective network to develop in the P3HT matrix, facilitating percolation pathways for electron transport. Therefore, the charge transport is considerably enhanced by using the CdS nanorods with higher aspect ratio. The enhancement in carrier mobility can be accomplished by improving the CdS−P3HT interface without the involvement of surfactants. All of the above merits give a PCE to a level as high as 2.9%, albeit there is room for technical development not yet being fully explored and optimized in terms of dimensional control of the nanorods and device assembly in this investigation. The results offer significant practical advantages in CdS nanorod-based solar cell device compared to those solar cells reported via the use of conventional hybrid composites.

Acknowledgment. This work was financially supported by the National Science Council of the Republic of China, Taiwan, under Contract No. NSC-2113-M-009-027-MY2.

References and Notes

(1) Coakley, K. M.; McGehee, M. D. *Chem. Mater.* **2004**, *16*, 4533.
(2) Cui, D.; Xu, J.; Zhu, T.; Paradee, G.; Ashok, S.; Gerhold, M. *Appl. Phys. Lett.* **2006**, *88*, 183111.
(3) Huynh, W. U.; Dittmer, J. J.; Alivisatos, A. P. *Science* **2002**, *295*, 2425.
(4) Zhang, S.; Cyr, P. W.; McDonald, S. A.; Kostantatos, G.; Sargent, E. H. *Appl. Phys. Lett.* **2005**, *87*, 233101.
(5) Watt, A. A. R.; Blake, D.; Warner, J. H.; Thomsen, E. A.; Tavenner, E. L.; Rubinsztein-Dunlop, H.; Meredith, P. *J. Phys. D* **2005**, *38*, 2006.
(6) Beek, W. J. E.; Wienk, M. M.; Kemerink, M.; Yang, X. N.; Janssen, R. A. J. *J. Phys. Chem. B* **2005**, *109*, 9505.
(7) Kang, Y.; Park, N.; Kim, D. *Appl. Phys. Lett.* **2005**, *86*, 113101.
(8) Arango, A. C.; Johnson, L. R.; Bliznyuk, V. N.; Schlesinger, Z.; Carter, S. A.; Hörhold, H.-H. *Adv. Mater.* **2000**, *12*, 1689.
(9) Li, W.; Liu, Y. S.; Xi, J.; Qin, D. H.; Cao, Y. *J. Phys. Chem. C* **2007**, *111*, 9538.
(10) Matsumura, M.; Saho, Y.; Tsubomura, H. *J. Phys. Chem.* **1983**, *87*, 3807.
(11) Lee, S. M.; Jun, Y. W.; Cho, S. N.; Cheon, J. *J. Am. Chem. Soc.* **2002**, *124*, 11244.
(12) Lee, S. M.; Cho, S. N.; Cheon, J. *Adv. Mater.* **2003**, *15*, 441.
(13) Joo, J.; Na, H. B.; Yu, T.; Yu, J. H.; Kim, Y. W.; Wu, F.; Zhang, J. Z.; Hyeon, T. *J. Am. Chem. Soc.* **2003**, *125*, 11100.
(14) Watt, A.; Thomsen, E.; Meredith, P.; Rubinsztein-Dunlop, H. *Chem. Commun.* **2004**, 2334.
(15) Watt, A.; Meredith, P.; Riches, J. D.; Atkinson, S.; Rubinsztein-Dunlop, H. *Curr. Appl. Phys.* **2004**, *4*, 320.
(16) Adelung, R.; Aktas, O. C.; Franc, J.; Biswas, A.; Kunz, R.; Elbahri, M.; et al. *Nat. Mater.* **2004**, *3*, 375.
(17) Yang, Q.; Tang, K.; Wang, C.; Qian, Y.; Zhang, S. *J. Phys. Chem. B* **2002**, *106*, 9227.
(18) Zhan, J.; Yang, X.; Wang, D.; Li, S.; Xie, Y.; Xia, Y.; et al. *Adv. Mater.* **2000**, *12*, 1348.
(19) Xie, Y.; Qiao, Z. P.; Chen, M.; Liu, X. M.; Qian, Y. T. *Adv. Mater.* **1999**, *11*, 1512.
(20) Niu, H.; Zhang, L.; Gao, M.; Chen, Y. *Langmuir* **2005**, *21*, 4205.
(21) Yang, C.-S.; Awschalom, D. D.; Stucky, G. D. *Chem. Mater.* **2002**, *14*, 1277.
(22) Gur, I.; Fromer, N. A.; Geier, M. L.; Alivisatos, A. P. *Science* **2005**, *310*, 462.
(23) Sun, B.; Greenham, N. C. *Phys. Chem. Chem. Phys.* **2006**, *8*, 3557.
(24) Savenije, T. J.; Kroeze, J. E.; Yang, X.; Loos, J. *Thin Solid Films* **2006**, *511*, 2.
(25) Rughooputh, S. D. D. V.; Hotta, S.; Heeger, A. J.; Wudl, F. *J. Polym. Sci., Polym. Phys. Ed.* **1987**, *25*, 1071.
(26) Stavrinadis, A.; Beal, R.; Smith, J. M.; Assender, H. E.; Watt, A. A. R. *Adv. Mater.* **2008**, *20*, 3105.
(27) Chen, F.; Zhou, R.; Yang, L.; Shi, M.; Wu, G.; Wang, M.; Chen, H. *J. Phys. Chem. C* **2008**, *112*, 13457.
(28) Wankhede, M. E.; Haram, S. K. *Chem. Mater.* **2003**, *15*, 1296.
(29) Sun, H.; Li, X.; Chen, Y.; Li, W.; Li, F.; Liu, B.; Zhang, X. *Nanotechnology* **2008**, *19*, 225601.
(30) Ginger, D. S.; Greenham, N. C. *Phys. Rev. B* **1999**, *59*, 10622.
(31) Greenham, N. C.; Peng, X.; Alivisatos, A. P. *Phys. Rev. B* **1996**, *54*, 17628.
(32) Yu, G.; Heeger, A. J. *J. Appl. Phys.* **1995**, *78*, 4510.
(33) Yu, J.; Hu, D. H.; Barbara, P. F. *Science* **2000**, *289*, 1327.
(34) Scholes, G. D.; Larsen, D. S.; Fleming, G. R.; Rumbles, G.; Burn, P. L. *Phys. Rev. B* **2000**, *61*, 13670.
(35) Koster, L. J. A.; Mihailetchi, V. D.; Ramaker, R.; Blom, P. W. M. *Appl. Phys. Lett.* **2005**, *86*, 123509.
(36) Brabec, C. J.; Cravino, A.; Meissner, D.; Sariciftci, N. S.; Fromherz, T.; Rispens, M. T.; Sanchez, L.; Hummelen, J. C. *Adv. Funct. Mater.* **2001**, *11*, 374.